

## THE STAR FORMATION RATE OF SUPERSONIC MHD TURBULENCE

PAOLO PADOAN,

Department of Physics and Center for Astrophysics and Space Sciences, University of California, San Diego,  
9500 Gilman Drive, La Jolla, CA 92093-0424; ppadoan@ucsd.edu

ÅKE NORDLUND

Niels Bohr Institute, University of Copenhagen, Juliane Maries Vej 30, DK-2100, Copenhagen, Denmark; aake@nbi.dk

*Submitted to ApJ Letters, March 11, 2019*

### ABSTRACT

This work revisits the star formation rate (SFR) model of Krumholz and McKee, extends it to the case of a magnetized medium, and verifies it with a set of numerical simulations of driven, supersonic, magneto-hydrodynamic (MHD) turbulence, where collapsing cores are captured with accreting sink particles. The main results are: i) a new physical interpretation of the critical density for star formation not based on the concepts of turbulent pressure support and sonic scale; ii) the derivation of the critical density in the MHD case and the derivation of the corresponding MHD model of the SFR, predicting a lower SFR and a stronger dependence on the virial parameter than the hydrodynamic (HD) model; iii) the demonstration that driven supersonic turbulence results in a constant SFR, after an initial transient phase with increasing SFR; iv) the derivation of the SFR in the simulations as a function of the virial parameter, shown to agree well with the SFR predicted by the MHD model, and less with the prediction of the HD model, potentially due to the important role of the Kelvin-Helmholtz instability of postshock shear layers in the HD case. A physical model of the SFR is needed for implementing the star formation feedback in simulations of galaxy formation. We suggest that the new star formation law derived in this paper be implemented in future galaxy formation simulations.

*Subject headings:* ISM: kinematics and dynamics – MHD – stars: formation – turbulence

### 1. INTRODUCTION

While many theoretical models have been advanced to explain the stellar initial mass function (IMF), relatively little work has been dedicated to study the star formation rate (SFR) until recently. A physical theory of the SFR should explain why the star-formation process is slow, meaning that it converts only a few percent of the gas mass into stars in a free-fall time,  $\tau_{\text{ff}}$ , both on Galactic scale (Zuckerman & Palmer 1974; Williams & McKee 1997) and on the scale of individual clouds (Krumholz & Tan 2007). Several authors have proposed that the observed supersonic turbulence may be responsible for keeping the SFR low by providing turbulent pressure support against the gravitational collapse. For example, Bonazzola et al. (1987, 1992) presented a gravitational instability analysis that includes the effect of local turbulent pressure support; Krumholz & McKee (2005) defined the critical density for star formation based on the local turbulent pressure support of a Bonnor-Ebert sphere; Hennebelle & Chabrier (2008) proposed that the Salpeter stellar IMF is the result of the local turbulent pressure support. In all these works, the turbulent pressure is assumed to scale according to the velocity scaling of the turbulence, given by the observed Larson velocity-size relation (Larson 1981; Heyer & Brunt 2004) or by numerical simulations.

The concept of turbulent pressure support was introduced in the context of subsonic, small-scale turbulence by Chandrasekhar (1951). It applies when the two following conditions are satisfied,  $L \ll L_J$  and  $\sigma_v \ll C_S$ , where  $L$  is the length scale,  $L_J$  is the Jeans length,  $\sigma_v$  is the velocity dispersion, and  $C_S$  is the sound speed.

In the supersonic turbulence of star-forming regions, both conditions are violated. As a result, the turbulence in principle could trigger gravitational collapse, causing a large-scale compression rather than impede it. The turbulence is responsible for much of the complex and filamentary density structure observed in molecular clouds, and prestellar cores are likely assembled as the densest regions in this turbulent fragmentation process (Padoan et al. 2001). However, even if supersonic turbulence creates dense regions that are gravitationally unstable, it does so inefficiently, and its net effect on the large scale is that of suppressing star formation when the total turbulent kinetic energy exceeds the total gravitational energy.

The complexity of the star-formation process could therefore be reduced to a simple phenomenological model where the SFR depends primarily on the ratio of the turbulent kinetic energy,  $E_K$ , and the gravitational energy,  $E_G$ , of a star-forming region. This ratio is measured by the virial parameter introduced by Bertoldi & McKee (1992),

$$\alpha_{\text{vir}} \sim \frac{2E_K}{E_G} = \frac{5\sigma_{v,1D}^2 R}{GM}, \quad (1)$$

where  $\sigma_{v,1D}$  is the one-dimensional rms velocity,  $R$  and  $M$  the cloud radius and mass respectively, and  $G$  the gravitational constant, and it has been assumed the cloud is a sphere with uniform density. If the dynamical time is defined as the ratio of the cloud radius and the three-dimensional rms velocity,  $\tau_{\text{dyn}} = R/\sigma_{v,3D}$ , and using the standard definition of the free-fall time,  $\tau_{\text{ff}} = (3\pi/(32G\rho))^{1/2}$ , the virial parameter can be ex-

pressed as  $\alpha_{\text{vir}} = 0.7(\tau_{\text{ff}}/\tau_{\text{dyn}})^2$ .

Krumholz & McKee (2005) derived a theoretical model where the SFR is primarily controlled by the virial parameter. In this model, it is assumed that the gas mass above some critical density,  $\rho_{\text{cr}}$ , is gravitationally unstable, and the fraction of this unstable mass is computed assuming the gas density obeys a Log-Normal pdf (Nordlund & Padoan 1999). Following Padoan (1995), the critical density is defined through the comparison of the Jeans' length and the sonic-scale,  $\lambda_s$ , which is the scale where the turbulent velocity differences are of the order of the speed of sound. The critical density is equivalent to that of the critical Bonnor-Ebert mass of size  $\lambda_s$ . This model represents a great simplification of the star formation problem, because it circumvents any account of the dynamics of turbulence, by taking advantage of its end-result, the Log-Normal pdf of gas density. The idea of relying on the density pdf was also exploited in Padoan & Nordlund (2002, 2004) to explain the stellar IMF and the origin of brown dwarfs, and by Padoan (1995) to model the SFR.

The model of Krumholz & McKee (2005) was calibrated and tested using low-resolution SPH simulations by Vázquez-Semadeni et al. (2003). Because of the important role of turbulent energy in this model, low-resolution simulations are inadequate. They do not develop an inertial range of turbulence and are expected to produce a too large SFR – which they do, as recognized in a later paper, based on higher-resolution grid simulations, by some of the same authors (Vázquez-Semadeni et al. 2005). However, Krumholz & McKee (2005) estimated a rather low SFR from the simulations of Vázquez-Semadeni et al. (2003) by fitting only their early evolution. We argue this is a transient phase of accelerated SFR and should not be used to test the model. A new set of larger simulations is needed to properly test the theoretical models. Because the model does not include the effect of magnetic fields, it should be extended to magneto-hydrodynamic (MHD) turbulence, and this MHD model should also be tested with large simulations.

In this work, we propose an extension of the SFR model to MHD turbulence, and present a set of simulations, both with and without a magnetic field, to test the theoretical predictions. We find that the numerical results confirm our MHD model of the SFR. In the HD simulations, the dependence of the SFR on the virial parameter is steeper than predicted by the model, perhaps due to a complex effect of the Kelvin-Helmholtz instability of postshock shear layers in the HD case.

We also derive the critical density for star formation based on a different interpretation than in Krumholz & McKee (2005). Our physical interpretation does not require any reference to the sonic scale or to turbulent pressure support, but gives essentially the same critical density as in Krumholz & McKee (2005), so our HD model of the SFR is the same as Krumholz & McKee (2005). The extension to MHD, also based on our physical interpretation of the critical density, results in a new theoretical model that predicts a lower SFR and a stronger dependence on the virial parameter than the HD model.

## 2. CRITICAL DENSITY FOR THE HD CASE

In the hydrodynamic (HD) case, the main source of pressure in the postshock gas is the thermal pressure, so the shock jump conditions are given by the balance of thermal pressure and ram pressure:

$$\rho_{\text{HD}} c_s^2 = \rho_0 (v_0/2)^2, \quad (2)$$

where  $c_s$  is the sound speed,  $\rho_0$  and  $\rho_{\text{HD}}$  the preshock and postshock gas densities, and  $v_0/2$  the shock velocity. Because we use this equation to estimate a characteristic postshock density in the HD case,  $\rho_{\text{HD}}$ , we choose the mean gas density,  $\rho_0$ , as the preshock density, and half the rms velocity,  $v_0$ , as the shock velocity. Assuming an ensemble of eddies with a randomly oriented velocity of mean magnitude  $v_0$ , the average collision velocity is also  $v_0$ . However, the shock velocity is half of that average collision velocity because the postshock layer is confined by two shocks, each with velocity  $v_0/2$ . The characteristic density is then given by:

$$\rho_{\text{HD}} = \rho_0 \mathcal{M}_{\text{S},0}^2/4, \quad (3)$$

where  $\mathcal{M}_{\text{S},0}$  is the rms sonic Mach number, and the characteristic thickness,  $\lambda_{\text{HD}}$ , of the postshock layers is:

$$\lambda_{\text{HD}} = (\gamma L_0) 4/\mathcal{M}_{\text{S},0}^2, \quad (4)$$

where  $L_0$  is the size (e.g. the diameter for a sphere) of the system and  $\gamma L_0$ , with  $\gamma \leq 1$ , is the turbulence integral scale. Because the turbulence velocity scaling is approximately  $v \propto \ell^{1/2}$ , this characteristic thickness is practically scale-independent (it would have been the same if derived at any other scale, not only at the outer scale). The local condition for collapse is that  $\lambda \geq 2 R_{\text{BE}}$ , where  $R_{\text{BE}}$  is the Bonnor-Ebert radius. The critical density is therefore defined by

$$\lambda_{\text{HD}} = 2 R_{\text{BE}}(\rho_{\text{cr,HD}}). \quad (5)$$

Since the thickness is scale independent, this condition can be used to define a scale-independent critical density for collapse. The local density depends on the distribution of local shock velocity and preshock density and is known to follow a Log-Normal pdf (Vázquez-Semadeni 1994; Padoan et al. 1997; Nordlund & Padoan 1999; Ostriker et al. 2001; Li et al. 2004; Kritsuk et al. 2007; Beetz et al. 2008; Lemaster & Stone 2008; Federrath et al. 2008). So there is a finite probability that a region exceeds the critical density and undergoes collapse. Using the following expression for the Bonnor-Ebert radius (McKee & Ostriker 2007):

$$R_{\text{BE}} = 0.486 c_s / (G^{1/2} \rho^{1/2}), \quad (6)$$

where  $G$  is the gravitational constant, the critical density for collapse is given by:

$$\rho_{\text{cr,HD}}/\rho_0 = 0.0371 \gamma^{-2} \alpha_{\text{vir}} \mathcal{M}_{\text{S},0}^2, \quad (7)$$

where  $\alpha_{\text{vir}}$  is the virial parameter defined above in equation (1), and can be re-written as

$$\alpha_{\text{vir}} = 5v_0^2/(\pi G \rho_0 L_0^2), \quad (8)$$

assuming the system is a uniform sphere of radius  $L_0/2$ , mean gas density  $\rho_0$ , and three-dimensional rms turbulent velocity  $v_0$ .

The critical density defined by equation (7) has the same dependence on  $\alpha_{\text{vir}}$  and  $\mathcal{M}_{\text{S},0}$  as the critical density derived by Krumholz & McKee (2005), and so the SFR we derive in the HD case is essentially the same as in their work. However, the critical density has been derived here without any reference to turbulent pressure support and the sonic scale. On the contrary, our derivation is based on the turbulence as a trigger of local gravitational instabilities through its dynamical pressure.

By comparing the characteristic density,  $\rho_{\text{HD}}$ , to the critical density,  $\rho_{\text{cr,HD}}$ , one can define an average condition for star formation as

$$\rho_{\text{HD}}/\rho_{\text{cr,HD}} = 3.521 \gamma^2 \alpha_{\text{vir}}^{-1} \geq 1, \quad (9)$$

which implies  $\alpha_{\text{vir}} \leq 3.521 \gamma^2 = 0.43$ , where we have used  $\gamma = 0.35$  in the last equality (the same value adopted in the comparison with the simulations). As shown below, because of the broad, Log-Normal gas density pdf (assuming that the actual postshock density distribution is responsible for the high-density tail of the Log-Normal pdf) the SFR is a rather smooth function of  $\alpha_{\text{vir}}$ . In any case, the condition (9) illustrates the fact that the star formation rate is primarily controlled by the virial parameter, and probably more weakly by the Mach number.

In numerical simulations, the integral scale of the turbulence is somewhat smaller than the system size ( $\gamma < 1$ ). For example, in our simulations of supersonic turbulence driven in the range of wavenumbers  $1 \leq k \leq 2$  ( $k = 1$  corresponds to the box size),  $\gamma \approx 0.35$  (including a correction factor discussed in Wang & George (2002)). We adopt this value of  $\gamma$  when we compare the models with the simulations in §7. If star-forming regions are driven on very large scales, for example by the expansion of supernova remnants (Korpi et al. 1999; Kim et al. 2001; de Avillez & Breitschwerdt 2005; Joungh & Mac Low 2006; de Avillez & Breitschwerdt 2007; Tamburro et al. 2009), the turbulence integral scale could be much larger than the size of individual star-forming regions. However, in our model  $\gamma L_0$  is the characteristic scale of regions of compression with velocity of order the flow rms velocity,  $v_0$ , with  $v_0$  measured within the region of size  $L_0$ . We therefore adopt the same value of  $\gamma = 0.35$  as estimated in the simulations. With  $\gamma = 0.35$ , the critical density becomes:

$$\rho_{\text{cr}}/\rho_0 = 0.303 \alpha_{\text{vir}} \mathcal{M}_{\text{S},0}^2. \quad (10)$$

With characteristic parameters of molecular clouds on a scale of 10 pc,  $\alpha_{\text{vir}} \approx 1.6$ ,  $\rho_0 \approx 200 \text{ cm}^{-3}$ , and  $\mathcal{M}_{\text{S},0} \approx 25$ , we get a characteristic density of  $\rho_{\text{HD}} \approx 3.1 \times 10^4 \text{ cm}^{-3}$  from equation (3), just a factor of two below the critical density,  $\rho_{\text{cr,HD}} \approx 303 \rho_0 \approx 6.06 \times 10^4 \text{ cm}^{-3}$ . These are reasonable densities for prestellar cores. The critical overdensity factor of 303 is only 10% larger than the value of 275 derived from equation (27) of Krumholz & McKee (2005), using the same values of  $\alpha_{\text{vir}}$  and  $\mathcal{M}_{\text{S},0}$  (notice that their Mach number is 1D, so a factor of  $3^{1/2}$  smaller than ours) and assuming  $\phi_x = 1.12$  for their numerical coefficient (their best fit to numerical simulations).

### 3. CRITICAL DENSITY FOR THE MHD CASE

We now consider the MHD case. For simplicity, we neglect thermal pressure and assume that magnetic pressure is dominant in the postshock gas, a good approximation also in a super-Alfvénic regime (the average ratio of postshock magnetic pressure to thermal pressure in our MHD simulations is  $1/\beta = 2.22$ ). The inclusion of thermal pressure would slightly reduce the critical density<sup>1</sup> and slightly increase the SFR. However, given the phenomenological nature of the model and its success in predicting the SFR of the MHD simulations (see §7), we prefer to keep it simple and neglect thermal pressure.

The jump conditions are then:

$$(1/2) \rho_{\text{MHD}} v_{\text{A}}^2 = \rho_0 (v_0/2)^2, \quad (11)$$

where  $v_{\text{A}}$  is the Alfvén velocity in the postshock gas defined by the postshock magnetic field perpendicular to the direction of compression. Because the field is amplified only in the direction perpendicular to the compression, the postshock perpendicular field is comparable to the total postshock field, and we can write,  $v_{\text{A}} \approx B/(4\pi\rho)^{1/2}$ , where  $B$  is the postshock magnetic field and  $\rho$  the postshock gas density. The characteristic gas density and the thickness of postshock layers is therefore:

$$\rho_{\text{MHD}} = \rho_0 (v_0/v_{\text{A}})^2/2, \quad (12)$$

and

$$\lambda_{\text{MHD}} = (\gamma L_0) 2/(v_0/v_{\text{A}})^2. \quad (13)$$

The value of  $\lambda_{\text{MHD}}$  is not scale independent. Indeed, its scale dependence is at the heart of the relation between the exponent of the Salpeter stellar IMF and the turbulent velocity power spectrum, in the IMF model of Padoan and Nordlund (2002). However, we can still define a characteristic thickness, and hence a characteristic critical density, as in the HD case, because the average postshock Alfvén velocity,  $v_{\text{A}}$ , does not depend on density. In numerical simulations of supersonic and super-Alfvénic turbulence, it is found that, although  $v_{\text{A}}$  has a very large scatter for any given density, its mean value is density independent, corresponding to a mean relation  $B \propto \rho^{1/2}$  (Padoan & Nordlund 1999). Zeeman splitting measurements of the magnetic field strength in molecular cloud cores are also consistent with an average value of  $v_{\text{A}}$  independent of density (Crutcher 1999). We can therefore use this density-independent average value of  $v_{\text{A}}$  and introduce an average, density-independent ratio of gas to magnetic pressures,  $\beta = 2 c_{\text{S}}^2/v_{\text{A}}^2$ . The thickness is then:

$$\lambda_{\text{MHD}} = (4\gamma L_0/\beta) / \mathcal{M}_{\text{S},0}^2 \quad (14)$$

Next we define the characteristic critical density for collapse by the balance of magnetic and gravitational energies for a sphere of radius  $\lambda_{\text{MHD}}/2$  and uniform magnetic field:

$$(1/2) v_{\text{A}}^2 = (3/5) G (4/3) \pi (\lambda_{\text{MHD}}/2)^2 \rho_{\text{cr,MHD}} \quad (15)$$

Using equation (14), equation (15) gives the following characteristic critical density for collapse:

$$\rho_{\text{cr,MHD}}/\rho_0 = (1/16) (\beta/\gamma^2) \alpha_{\text{vir}} \mathcal{M}_{\text{S},0}^2 \quad (16)$$

<sup>1</sup> The increased thickness of postshock layers has a stronger effect than the increased pressure support against gravity, as one can see from equation (15).

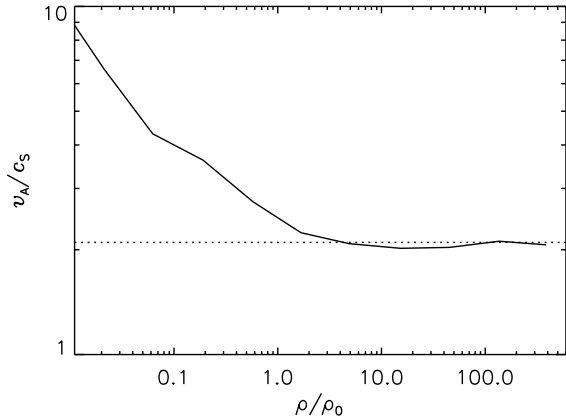


FIG. 1.— Mean Alfvén velocity, in units of the sound speed, versus gas density, in units of the mean density. The Alfvén velocity is essentially independent of density for densities above the mean. The dotted line shows the mean value of 0.21, computed for densities larger than twice the mean.

This critical density is almost the same as in the HD case, depending on the specific value of  $\beta$ ,  $\rho_{\text{cr,MHD}}/\rho_{\text{cr,HD}} = 1.68\beta$ . We have verified that the average value of  $\beta$  is independent of density in the MHD simulation used to generate the initial condition for the MHD star-formation simulations described in §6. In that simulation, the rms sonic Mach number is  $\mathcal{M}_{\text{S},0} \approx 9$  and the mean Alfvén velocity  $v_{\text{A},0} = 0.3 c_{\text{S}}$ , computed with the mean density and mean magnetic field. However, the rms magnetic field is amplified by the turbulence, so the actual Alfvén velocity should be computed as the *local* absolute value of  $B$  divided by the *local* value of the density, which gives,  $v_{\text{A}} = |B|/(4\pi\rho)^{1/2} = 2.1 c_{\text{S}}$ , if averaged over all regions with density larger than twice the mean (the Alfvén velocity introduced in eq. (11) is measured in the postshock gas, so it should be estimated as an average in over-dense regions). Figure 1 shows the mean Alfvén velocity conditioned to gas density in the snapshot used as the initial condition for the MHD star-formation simulations (see § 6). The Alfvén velocity is almost exactly constant at densities above the mean. The derived mean Alfvén velocity corresponds to a value of  $\beta = 0.45$ . With this specific value of  $\beta$ ,  $\rho_{\text{cr,MHD}}/\rho_{\text{cr,HD}} = 0.76$  and star formation should be more likely in MHD turbulence than in the HD case. However, due to the less broad gas density pdf in the MHD case discussed in the next section, the net result is a lower SFR than in the HD case.

#### 4. GAS DENSITY PDF

Because we have determined a characteristic critical density for local collapse, we can estimate the gas mass fraction that is turned into stars by computing the mass fraction above the critical density, as in Krumholz & McKee (2005). For a given virial parameter and Mach number (hence a given critical density), this mass fraction is controlled by the density pdf. In the HD case the density pdf is known to be Log-Normal, with a standard deviation depending on the rms Mach number. Following the numerical results in Padoan et al. (1997) for the Mach number dependence, the pdf is given

by:

$$p(x)dx = \frac{x^{-1}}{(2\pi\sigma^2)^{1/2}} \exp\left[-\frac{(\ln x - \langle \ln x \rangle)^2}{2\sigma^2}\right] dx \quad (17)$$

where  $x$  is the overdensity with respect to the mean density  $\rho_0$ ,  $x = \rho/\rho_0$ , the mean of the logarithm of the density is given by

$$\langle \ln x \rangle = -\frac{\sigma^2}{2} \quad (18)$$

and its standard deviation,  $\sigma$ , by

$$\sigma^2 \approx \ln\left[1 + \left(\frac{\mathcal{M}_{\text{S},0}}{2}\right)^2\right] \quad (19)$$

Notice that equation (19) for the standard deviation of the logarithm of the overdensity,  $\ln x$ , implies a simple relation for the standard deviation of the overdensity,  $\sigma_x$ ,

$$\sigma_x \approx \mathcal{M}_{\text{S},0}/2 \quad (20)$$

In the MHD case the density pdf may deviate from the Log-Normal and it may depend on both the sonic and the Alfvénic Mach numbers. Lemaster & Stone (2008) have shown that the density pdf in supersonic MHD simulations with a strong field, corresponding to a mean value of  $\beta_0 = 0.02$ , is very similar to the density pdf in the HD case. However, their study only applies to the relation between the mean of the pdf and the sonic Mach number. It does not provide estimated values of the rms density or of the postshock Alfvén velocity (introduced in our equation (11)), needed to estimate the value of  $\beta$  that enters our formulae. In the absence of a set of simulations with different values of the mean magnetic field, here we derive a simple model for the density pdf in the MHD case, based on arguments inspired by the HD case.

We assume that the pdf can be approximated by a Log-Normal also in the MHD case, at least in the super-Alfvénic regime that we think is relevant for molecular clouds (Padoan and Nordlund 1999; Lunttila et al. 2008,2009). This may not be a good approximation for the low density tail of the pdf, but for the present purpose we are primarily interested in the high density tail. To derive an expression for  $\sigma$  in the MHD case, we first show that the dependence of  $\sigma$  on  $\mathcal{M}_{\text{S},0}$  in the HD case can be obtained with a simple derivation, and we then apply the same derivation to the MHD case.

Let's consider a cubic box of size  $L_0$  swept by a single compression of sonic Mach number  $\mathcal{M}_{\text{S},0}$  in one direction and therefore accumulating all the mass in a postshock layer of size  $L_0$  and density and thickness given by equations (3) and (4) respectively, with  $\gamma = 1$ . The standard deviation of the density,  $\sigma_\rho$ , is given by

$$\sigma_\rho^2 = \frac{1}{V} \int_V (\rho - \rho_0)^2 dV \quad (21)$$

where  $V$  is the volume, and the integral is over the whole volume. In our simple model, the density is either zero outside of the layer, or  $\rho = \rho_{\text{HD}} \gg \rho_0$  inside the layer. The integral is therefore approximately equal to  $\rho_{\text{HD}}^2$  times the volume of the layer,  $V_{\text{layer}}$ :

$$\sigma_\rho^2 \approx \frac{1}{V} (\rho_{\text{HD}}^2 V_{\text{layer}}) = \frac{\lambda_{\text{HD}} L_0^2}{L_0^3} \rho_{\text{HD}}^2 = \rho_0^2 \mathcal{M}_{\text{S},0}^2 / 4 \quad (22)$$

where we have used equations (3) and (4) in the last equality. This result is equivalent to equation (20),  $\sigma_x \approx \mathcal{M}_{S,0}/2$ , which was derived from numerical simulations of supersonic turbulence (Padoan et al. 1997; Nordlund & Padoan 1999). Following the same derivation in the MHD case we obtain:

$$\sigma_{x,\text{MHD}} \approx \beta^{1/2} \mathcal{M}_{S,0}/2 \quad (23)$$

As mentioned above, in our simulation with  $\mathcal{M}_{S,0} \approx 9$

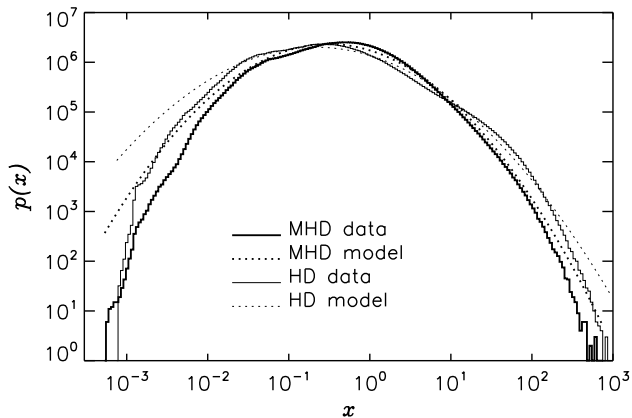


FIG. 2.— Pdf of gas density for the MHD and HD snapshots used as initial conditions for the star-formation simulations (solid lines). The Log-Normal models used in this work are also shown (dotted lines).

and mean Alfvén velocity  $v_{A,0} = 0.3 c_S$  (computed with the mean density and mean magnetic field), we get an average value of the postshock gas to magnetic pressures equal to  $\beta = 0.45$  (averaged over all regions with density larger than twice the mean), and find that this value is almost independent of density, for densities larger than the mean. According to our equation (23), in that super-Alfvénic simulation we should therefore obtain  $\sigma_{x,\text{MHD}} \approx 2.9$ . The actual value in the simulation is 2.7 (computed directly from the density field, not from a fit to the density pdf), very close to the prediction of our simple model. Figure 2 compares the HD and MHD model pdfs to the actual pdfs of the snapshots used as initial conditions for the star-formation simulations. The MHD model provides an excellent fit to the high density tail of the pdf, for almost 4 orders of magnitude in probability. At the highest densities the model predicts a slightly larger probability, a discrepancy that may be attributed to the limited numerical resolution. The pdf from the HD snapshot also lies below the model pdf at the highest densities.

The compilation of OH and CN Zeeman measurements by Troland & Crutcher (2008) and Falgarone et al. (2008) give an average value of  $\beta = 0.39$ , independent of density (the value is the same in the two samples, even if the mean gas density of the CN cores is approximately two orders of magnitude larger than that of the OH cores), in very close agreement with the results of our super-Alfvénic simulation. Observations give the magnetic field and the value of  $\beta$  in dense regions, so the observational  $\beta$  corresponds to the postshock  $\beta$  defined here. It would be hard to estimate the mean magnetic

field from observations over a large volume, because the Zeeman splitting of emission or absorption lines cannot be detected in low density regions. In numerical simulations of super-Alfvénic turbulence, the rms magnetic field is the result of the amplification of some weak initial field by compressions and, possibly, by a turbulent dynamo. These simulations typically start from an initially uniform field,  $B_0$ , which is also the conserved mean magnetic field. It would therefore be useful to relate  $\beta$  to the gas to magnetic pressure computed with the mean magnetic field,  $B_0$ , and the mean gas density,  $\rho_0$ ,  $\beta_0 = 2 c_S^2 / v_{A,0}^2$ . This relation will be studied in a future work, while here we will only refer to  $\beta$  in our formulae.

## 5. STAR FORMATION RATE

In Padoan & Nordlund (2004) we computed the mass fraction available to form brown dwarfs as the integral of the pdf of gas density from a critical density to infinity. In that case the critical density was defined as the density of a critical Bonnor-Ebert sphere with a mass of  $0.075 M_\odot$ . Krumholz & McKee (2005) used the same integral to compute the total mass available for star formation, and defined the critical density based on the condition of turbulent support of a Bonnor-Ebert sphere. Here we follow the same procedure, but our critical density is defined as the density of a critical Bonnor-Ebert sphere (or a critical magnetized sphere) of diameter equal to the characteristic postshock layer thickness. As shown above, our critical density in the HD case has the same dependence on  $\alpha_{\text{vir}}$  and  $\mathcal{M}_{S,0}$  and almost the same numerical value as the critical density derived by Krumholz & McKee (2005).

Assuming that the mass fraction above the critical density is turned into stars in a free-fall time of the mean density,  $\rho_0$ , as in Krumholz & McKee (2005), the star formation rate per free-fall time (the mass fraction turned into stars in a free-fall time) is given by:

$$\text{SFR}_{\text{ff}} = \int_{x_{\text{cr}}}^{\infty} x p(x) dx = \frac{1}{2} + \frac{1}{2} \text{erf} \left[ \frac{\sigma^2 - 2 \ln(\rho_{\text{cr}}/\rho_0)}{2^{3/2} \sigma} \right] \quad (24)$$

where  $x_{\text{cr}} = \rho_{\text{cr}}/\rho_0$ . The choice of expressing the SFR with a time unit equal to the free-fall time, introduced in Krumholz & McKee (2005), is useful when comparing with observational data, because it turns out that the value of  $\text{SFR}_{\text{ff}}$  is approximately the same in very different star-formation environments, as shown by Krumholz & Tan (2007).

Because  $\rho_{\text{cr}}$  is derived as an average critical density, the integral in equation (24) is justified only if the actual local value of the critical density does not correlate with the local value of the density. This requires that local values of postshock layer density,  $\rho$ , and thickness,  $\lambda$ , are not correlated with each other. Both  $\rho$  and  $\lambda$  depend on the local shock velocity, so one may expect them to have correlated fluctuations around their mean values. However, the shock velocity varies not only because of random fluctuations at a fixed scale, but also because they increase with scale, being approximately proportional to  $L^{1/2}$ . As discussed above, the characteristic thickness is scale-independent, so the range in shock velocity introduced by the range in velocity due the scaling does not generate any correlation between the local

density and the local critical density. Therefore, if the range in shock velocities due to its scaling dominates over the range in local shock velocity due to fluctuations at a fixed scale, the mean value of the critical density will not show any correlation with the local density, and the integral in equation (24) is justified.

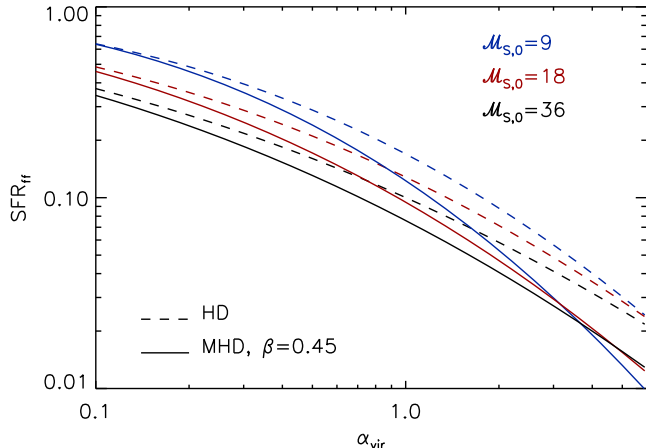


FIG. 3.— The star formation rate per free-fall time versus the virial parameter according to equation (24), for the HD case (dashed lines), and the MHD case (solid lines). The solid lines are for  $\beta = 0.45$ , as in our MHD simulations, and consistent with OH Zeeman splitting measurements in cloud cores. In both cases, the three lines are for three different values of the sonic rms Mach number,  $\mathcal{M}_{S,0} = 9, 18, 36$ , from top to bottom respectively.

Figure 3 shows the result of equation (24) as a function of the virial parameter, for three values of the sonic Mach number,  $\mathcal{M}_{S,0} = 9, 18, 36$ , in the MHD case with  $\beta = 0.45$ , as discussed in §2. For  $\alpha_{\text{vir}} < 3$  in the MHD case and  $\alpha_{\text{vir}} < 6$  in the HD case, the SFR decreases with increasing Mach number. The SFR is not very sensitive to the Mach number, because as the Mach number and the critical density increase, the standard deviation of the gas density pdf also increases. In the HD case and in the MHD case with  $\beta = 0.45$ , the dependence is approximately  $\text{SFR}_{\text{ff}} \sim \mathcal{M}_{S,0}^{0.4}$  at very low values of  $\alpha_{\text{vir}}$ , and becomes weaker at increasing values of the virial parameter, consistent with Figure 3 in Krumholz & McKee (2005) and with the power-law approximation in their equation (30).

As mentioned above, OH and CN Zeeman measurements in molecular cloud cores yield an average value of  $\beta = 0.39$ , independent of density (Troland & Crutcher 2008; Falgarone et al. 2008). Assuming this observed value for the postshock  $\beta$ , a value of  $\mathcal{M}_{S,0} = 25$ , representative of molecular clouds on a scale of approximately 10 pc, and  $\alpha_{\text{vir}} = 1.6$ , appropriate for average density-size and velocity-size Larson’s relations, we get an average value of  $\text{SFR}_{\text{ff}} \approx 0.05$ . If a factor of approximately 0.3 of the mass of a prestellar core goes into the final star, as suggested by Krumholz et al. (2009), then we predict an average SFR per free-fall time of approximately 1.5% in molecular clouds obeying average Larson’s relations, as typically observed.

In order to test the SFR model, we have run a set of simulations of driven supersonic turbulence, on meshes with  $500^3$ -  $1,000^3$  computational zones. Using the same methods and setup as in Padoan & Nordlund (2002) and Padoan & Nordlund (2004) we adopt periodic boundary conditions, isothermal equation of state, random forcing in Fourier space at wavenumbers  $1 \leq k \leq 2$  ( $k = 1$  corresponds to the computational box size), uniform initial density and magnetic field, random initial velocity field with power only at wavenumbers  $1 \leq k \leq 2$ . The simulations are all based on two initial snapshots of fully developed turbulence, one for HD and one for MHD. These initial snapshots are obtained by running the HD and the MHD simulations for approximately 5 dynamical times, on meshes with  $1,000^3$  computational zones, with the driving force keeping the rms sonic Mach number at the approximate value of  $\mathcal{M}_{S,0} = \sigma_{v,3D}/c_S \approx 9$ .

In the MHD simulation, the initial magnetic field is such that the initial value of the ratio of gas to magnetic pressure is  $\beta_0 = 22.2$ . At the time when the gravitational force is included, the magnetic field has been amplified by the turbulence, and the value of  $\beta$  defined as  $\beta = 2c_S^2/(|B|/(4\pi\rho)^{1/2})^2$  and averaged over regions with gas density larger than twice the mean (our definition of the postshock beta), is  $\beta = 0.45$ . Finally, using the rms magnetic field and the mean density, we can define a value of  $\beta_{\text{rms}} = 0.2$ , corresponding to an rms Alfvénic Mach number of  $\mathcal{M}_A \approx 4$ .

The star formation simulations start when the gravitational force is included by specifying a value of the gravitational parameter. As the gravitational force is included, the computational mesh is downsized from  $1,000^3$  to  $500^3$  zones. Table 1 gives the corresponding values of the Jeans length in units of the box size,  $L_J/L_0 \approx 1.94 \alpha_{\text{vir}}^{1/2} \mathcal{M}_{S,0}^{-1}$ , for all 10 simulations with an rms sonic Mach number  $\mathcal{M}_{S,0} = 9$  (3 HD runs and 7 MHD runs). The driving force is still active during the star-formation simulations, in order to achieve a stationary value of  $\alpha_{\text{vir}}$  and a well-defined, constant SFR.

Our simulations represent an intermediate range of scales. The forcing represents the inertial forcing from scales larger than the box size. These larger scale motions have longer turn-over times – and hence longer life times – than the turn-over times of the scales covered by the simulations. They act to maintain the kinetic energy on smaller scales. Without the corresponding driving, the motions on the scales covered by the simulations would decay, which would lead to a lowering of the virial parameter and a corresponding secular increase in the star formation rate. By maintaining the driving we avoid the secular evolution and obtain a consistent and nearly constant star formation rate.

Table 1 also gives the values of the virial parameter,  $\alpha_{\text{vir}}$ , assuming the rms Mach number  $\mathcal{M}_{S,0} = 9$ . The virial parameter defined in equation (1) is for a sphere of uniform density. The simulations are carried out in a cubic domain and generate a highly nonlinear density field; real star-forming regions have irregular shapes and are highly fragmented. The virial parameter of the simulations, as well as that of real molecular clouds, is therefore only an approximation of the energy ratio. For the simulations, in the formula defining the virial parameter we use  $R = L/2$ , where  $L$  is the box size. In this way the

TABLE 1  
NON-DIMENSIONAL PARAMETERS FOR SIMULATIONS WITH RMS  
SONIC MACH NUMBER  $\mathcal{M}_{S,0} = 9$

Run	$N$	$\beta$	$L_J/L_0$	$\alpha_{\text{vir}}$	$\text{SFR}_{\text{ff}}$
HD1	$1,000^3 \rightarrow 500^3$	$\infty$	0.18	0.67	0.59
HD2	$1,000^3 \rightarrow 500^3$	$\infty$	0.31	2.04	0.13
HD3	$1,000^3 \rightarrow 500^3$	$\infty$	0.46	4.51	0.02
MHD1	$1,000^3 \rightarrow 500^3$	0.45	0.10	0.20	0.42
MHD2	$1,000^3 \rightarrow 500^3$	0.45	0.12	0.33	0.30
MHD3	$1,000^3 \rightarrow 500^3$	0.45	0.15	0.47	0.24
MHD4	$1,000^3 \rightarrow 500^3$	0.45	0.18	0.67	0.17
MHD5	$1,000^3 \rightarrow 500^3$	0.45	0.21	0.95	0.11
MHD6	$1,000^3 \rightarrow 500^3$	0.45	0.25	1.35	0.06
MHD7	$1,000^3 \rightarrow 500^3$	0.45	0.31	2.04	0.03

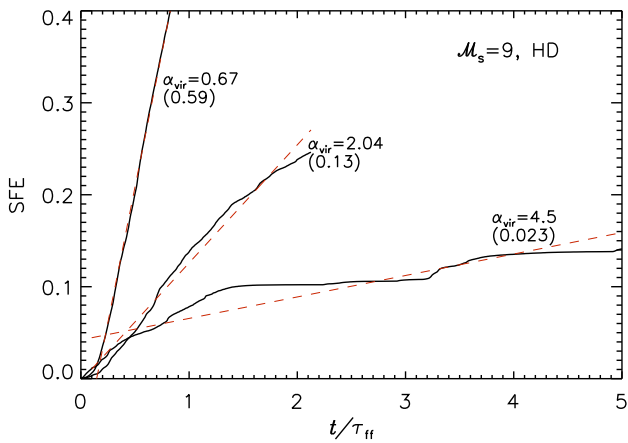


FIG. 4.— Star-formation efficiency versus time for the three HD star-formation simulations. The efficiency is defined as the mass in stars (sink particles) divided by the total mass, and the time is in units of the free-fall time in each simulation. The dashed lines show the least-squares fit to each curve (starting at  $t = 0.4\tau_{\text{ff}}$ ). The slope of those linear fits defines the  $\text{SFR}_{\text{ff}}$ , given in parenthesis below the value of  $\alpha_{\text{vir}}$ .

virial parameter is very close to the energy ratio in the case of a cube of uniform density.

A collapsing region is captured by the creation of an accreting sink particle if the density exceeds a certain density threshold (4,000 and 16,000 times the mean density in the  $500^3$  and  $1000^3$  cases, respectively). We have verified that the largest density reached by non-collapsing regions is always much smaller than that value, so only a collapsing region can create a sink particle. No other conditions need to be satisfied to identify genuine collapsing regions. Once a particle is created its subsequent motion is followed, allowing for influences from the gravitational potential and from accretion. When calculating the gravitational potential the masses of the stars are added back into a fiducial density field, using narrow Gaussian profiles ( $1/e$  radius 1.15 grid zones) to represent the sink particles. The Poisson equation for the gravitational potential is solved using parallelized Fast Fourier Transforms with Gaussian softening ( $1/e$  radius  $2\sqrt{2}$  grid zones).

Further accretion (defined as density exceeding the density threshold) is collected onto the nearest sink particle if the distance is less than four grid zones. Sink particles are not merged, and thus maintain their iden-

tity even if they become trapped in the same potential well (the softening of the gravitational potential ensures that no singularity occurs).

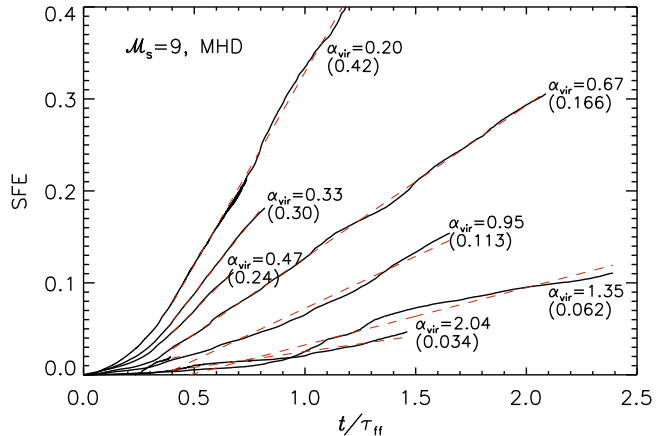


FIG. 5.— Same as Figure 4, but for the seven MHD star-formation simulations.

In Figures 4 and 5 we show the star formation efficiency (SFE) versus time in the HD and MHD simulations respectively. The SFE is defined as the mass in sink particles divided by the total initial mass. The time is given in units of the free-fall time of each simulation, so the slope of the plots corresponds to the  $\text{SFR}_{\text{ff}}$ . The plots only show the SFE from the time when the first sink particle is created, which is some time after the gravity is turned on. The time to the formation of the first sink particles is longer for simulations with larger  $\alpha_{\text{vir}}$ , which cannot be seen in Figures 4 and 5. Especially in the MHD case, even after the first sink particle is created, there is still an initial transient phase with increasing SFR. This transient phase usually does not last for more than  $0.4\tau_{\text{ff}}$  after the first sink particle is created. The  $\text{SFR}_{\text{ff}}$  is therefore estimated as the slope of a least-square fit to the SFE after  $0.4\tau_{\text{ff}}$  from the creation of the first sink particle. The HD and MHD runs with the lowest  $\alpha_{\text{vir}}$  were run until a very high value of the SFE was reached, but the least-square fit is only computed up to  $\text{SFE} \leq 0.4$ , because for even larger SFE the stars could gravitationally affect the turbulence, which is beyond the scope of this study.

Figures 4 and 5 show that the  $\text{SFR}_{\text{ff}}$  (given in parenthesis below the value of  $\alpha_{\text{vir}}$  and also in the last column of Table 1), decreases monotonically with increasing  $\alpha_{\text{vir}}$ . It is well defined because the SFE plots are almost straight lines (constant instantaneous SFR) for almost all the simulations, except for the HD run with the largest virial parameter,  $\alpha_{\text{vir}} = 4.5$ . With such a large value of the virial parameter the star formation is sporadic, with periods of almost no star formation lasting up to  $2\tau_{\text{ff}}$ .

## 7. MODELS VERSUS NUMERICAL RESULTS

Figure 6 compares the SFR models with the numerical results. It shows the  $\text{SFR}_{\text{ff}}$  versus  $\alpha_{\text{vir}}$  for all the simulations listed in Table 1 and for the HD and MHD models. The solid lines show the mass fraction above the critical density computed with the theoretical density pdf, while the dotted lines show the same quantity computed with the actual density pdf in the snapshots immediately pre-

ceding the inclusion of self-gravity (the same four pdfs shown in Figure 2). Given our limited resolution, and because the numerical pdf is from a single snapshot, the numerical pdf does not match the theoretical one exactly (as shown in Figure 2) and thus predicts a slightly different SFR. In the HD case for  $\alpha_{\text{vir}} > 1.3$ , and in the MHD case for all values of  $\alpha_{\text{vir}}$ , the dotted line is steeper

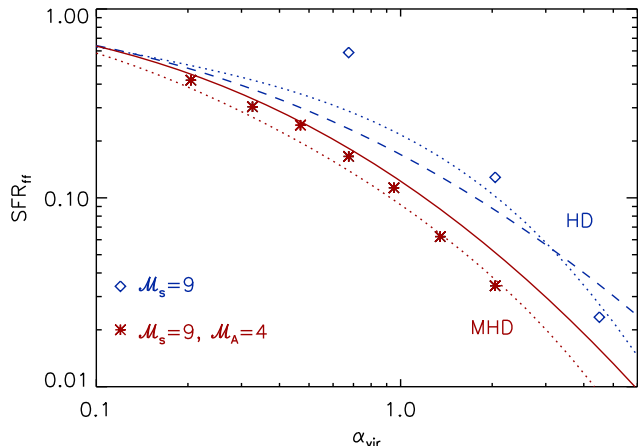


FIG. 6.— Star formation rate per free-fall time versus virial parameter for the MHD simulations (asterisk symbols) and for the HD simulations (diamond symbols). The solid lines are the corresponding model predictions based on the model density pdfs (see Figure 2). The dotted lines show the model predictions based on the actual pdfs in the snapshots immediately preceding the inclusion of self-gravity (see Figure 2).

than the solid one, because the high-density tails of the actual pdfs are slightly below the tails of the model pdfs, as shown in Figure 2, due to the finite numerical resolution.

The MHD simulations yield values of  $\text{SFR}_{\text{ff}}$  versus  $\alpha_{\text{vir}}$  matching the theoretical prediction extremely well. The theoretical plots show the mass fraction above the critical density without any vertical adjustment, meaning that we have not multiplied the theoretical mass fraction by any free parameter. The HD results agree well with the model prediction for the two largest values of  $\alpha_{\text{vir}}$ , especially in the case of the dotted line, corresponding to the model applied to the actual gas density pdf just before the inclusion of self-gravity. The run HD1, with  $\alpha_{\text{vir}} = 0.67$ , gives instead a  $\text{SFR}_{\text{ff}}$  approximately twice larger than predicted by the HD model.

We have not yet investigated the origin of this discrepancy. We suspect it may be related to the Kelvin-Helmholtz instability of postshock shear layers. The model assumes that the postshock gas can accumulate into dense layers. However, the shocks are in general oblique and create a shear flow in the postshock layers. In the HD case, this postshock shear flow is Kelvin-Helmholtz unstable (see § 3.7 in Kritsuk et al. 2007), which may cause the fragmentation of most postshock layers. The global effect of this fragmentation process on the SFR as a function of  $\alpha_{\text{vir}}$  is hard to predict. In the MHD case, magnetic tension tends to stabilize hydrodynamically unstable postshock shear layers (Miura & Pritchett 1982; Keppens et al. 1999; Keppens & Tóth 1999; Ryu et al. 2000; Baty & Keppens 2002; Baty et al. 2003), and therefore the MHD model does not require major corrections due to instabilities of

postshock layers.

## 8. SUMMARY AND CONCLUDING REMARKS

This work extends the SFR model of Krumholz & McKee (2005) by proposing an alternative physical interpretation of the origin of the critical density for star formation, and by deriving the SFR also for the case of a magnetized medium. In this new MHD model the SFR is predicted to be lower, and to have a steeper dependence on  $\alpha_{\text{vir}}$  than in the HD model. Both models have been tested with a set of numerical simulations of driven supersonic turbulence where the SFR is found to be nearly constant after an initial transient phase. The numerical MHD results follow closely the theoretical prediction, while in the HD simulations the  $\text{SFR}_{\text{ff}}$  versus  $\alpha_{\text{vir}}$  relation is steeper than in the HD SFR model, perhaps due to instabilities of the postshock shear layers not accounted for in the model.

Although based on reasonable physical assumptions, this phenomenological model of the SFR bypasses the great complexity of the nonlinear dynamics of supersonic and self-gravitating turbulence. For example, it does not truly explain why the characteristic time-scale should be the free-fall time of the mean density,  $\tau_{\text{ff},0}$ , instead of that of the critical density,  $\tau_{\text{ff},\text{cr}}$ . Unstable regions with  $\rho \geq \rho_{\text{cr}}$  would be expected to collapse within a time-scale of order  $\tau_{\text{ff},\text{cr}}$ . However, if  $\tau_{\text{ff},\text{cr}}$  were used as the characteristic time in the model, the SFR would be larger and would have a weaker dependence on  $\alpha_{\text{vir}}$ , which would not match the simulations. Such an alternative model could be made to match the simulations only by introducing an artificial efficiency factor, scaling like  $\alpha_{\text{vir}}^{-1/2}$ .

Our phenomenological model gives the correct  $\text{SFR}_{\text{ff}}$  versus  $\alpha_{\text{vir}}$  relation and offers an insight on the importance of turbulence in star formation. Because it provides a prediction of the SFR based solely on turbulence statistics, with no correction for the effect of self-gravity, it shows that the process of star formation may be envisioned as the effect of two almost independent steps: i) turbulent fragmentation, with little influence from self-gravity, and ii) the local collapse of the densest regions, with little influence from turbulence. This approximation is a basic assumption in the stellar IMF model of Padoan & Nordlund (2002) as well. It is also fundamentally different from the assumptions of star formation models relying on the concept of local turbulent pressure support, where the local competition between turbulence and self-gravity is always important on all scales.

This work illustrates how the turbulence controls the SFR. It does not address how the turbulence is driven to a specific value of  $\alpha_{\text{vir}}$ . Because much of the turbulence driving is likely due to SNa explosions on galactic scales (Korpi et al. 1999; Kim et al. 2001; de Avillez & Breitschwerdt 2005; Joung & Mac Low 2006; de Avillez & Breitschwerdt 2007; Tamburro et al. 2009), or HII regions on giant molecular cloud scales (Krumholz et al. 2009, 2006), the turbulent kinetic energy and the value of  $\alpha_{\text{vir}}$  are coupled to the SFR in a feedback loop. The feedback determines the equilibrium level of the SFR (and hence also the equilibrium level of  $\alpha_{\text{vir}}$ ) at large scales. If  $\alpha_{\text{vir}}$  were to decrease (increase) relative to the equilibrium the SFR would increase (decrease), according to the results of this work, resulting



in an increased (decreased) energy injection rate by SNA explosions, thus restoring a higher (lower) value of  $\alpha_{\text{vir}}$ . The rather strong dependence of the SFR on  $\alpha_{\text{vir}}$  found in this work suggests that this self-regulation may work quite effectively.

Cosmological simulations of galaxy formation provide the rate of gas cooling and infall, which sets the gas reservoir for the star formation process and thus ultimately controls the SFR. They also include prescriptions for the star formation feedback, known to be essential to recover observed properties of galaxies. Future galaxy formation simulations should adopt a physical SFR law with the correct dependence on  $\alpha_{\text{vir}}$  and  $\mathcal{M}_{\text{S},0}$  as derived in this work, in order to correctly reflect specific conditions of protogalaxies at different redshifts. This requires a treatment of the star formation feedback capable of providing

an estimate of  $\alpha_{\text{vir}}$  on scales of order 10-100 pc.

We are grateful to Liubin Pan, Chris McKee, and Mark Krumholz for reading the manuscript and providing useful comments. This research was supported in part by the NASA ATP grant NNG056601G, NSF grant AST-0507768, and a grant from the Danish Natural Science Research Council. This work was prepared in part during the workshop ‘Star Formation Through Cosmic Time’ at the KITP in Santa Barbara, and was supported in part by the National Science Foundation under Grant No. PHY99-07949. We utilized computing resources provided by the San Diego Supercomputer Center, by the NASA High End Computing Program, and by the Danish Center for Scientific Computing.

## REFERENCES

- Baty, H. & Keppens, R. 2002, *ApJ*, 580, 800  
 Baty, H., Keppens, R., & Comte, P. 2003, *Physics of Plasmas*, 10, 4661  
 Beetz, C., Schwarz, C., Dreher, J., & Grauer, R. 2008, *Physics Letters A*, 372, 3037  
 Bertoldi, F. & McKee, C. F. 1992, *ApJ*, 395, 140  
 Bonazzola, S., Falgarone, E., Heyvaerts, J., Perault, M., & Puget, J. L. 1987, *A&A*, 172, 293  
 Bonazzola, S., Perault, M., Puget, J. L., Heyvaerts, J., Falgarone, E., & Panis, J. F. 1992, *J. Fluid Mech.*, 245, 1  
 Chandrasekhar, S. 1951, *Proc. Roy. Soc.*, 210, 26  
 Crutcher, R. M. 1999, *ApJ*, 520, 706  
 de Avillez, M. A. & Breitschwerdt, D. 2005, *A&A*, 436, 585  
 de Avillez, M. A., & Breitschwerdt, D. 2007, *ApJ*, 665, L35  
 Falgarone, E., Troland, T. H., Crutcher, R. M., & Paubert, G. 2008, *A&A*, 487, 247  
 Federrath, C., Klessen, R. S., & Schmidt, W. 2008, *ApJ*, 688, L79  
 Hennebelle, P. & Chabrier, G. 2008, *ApJ*, 684, 395  
 Heyer, M. H. & Brunt, C. M. 2004, *ApJ*, 615, L45  
 Joung, M. K. R. & Mac Low, M.-M. 2006, *ApJ*, 653, 1266  
 Keppens, R. & Tóth, G. 1999, *Physics of Plasmas*, 6, 1461  
 Keppens, R., Tóth, G., Westermann, R. H. J., & Goedbloed, J. P. 1999, *Journal of Plasma Physics*, 61, 1  
 Kim, J., Balsara, D., & Mac Low, M.-M. 2001, *Journal of Korean Astronomical Society*, 34, 333  
 Korpi, M. J., Brandenburg, A., Shukurov, A., Tuominen, I., & Nordlund, Å. 1999, *ApJL*, 514, L99  
 Kritsuk, A. G., Norman, M. L., Padoan, P., & Wagner, R. 2007, *ApJ*, 665, 416  
 Krumholz, M. R., Matzner, C. D., & McKee, C. F. 2006, *ApJ*, 653, 361  
 Krumholz, M. R. & McKee, C. F. 2005, *ApJ*, 630, 250  
 Krumholz, M. R., McKee, C. F., & Tumlinson, J. 2009, *ApJ*, 699, 850  
 Krumholz, M. R. & Tan, J. C. 2007, *ApJ*, 654, 304  
 Larson, R. B. 1981, *MNRAS*, 194, 809  
 Lemaster, M. N. & Stone, J. M. 2008, *ApJ*, 682, L97  
 Li, P. S., Norman, M. L., Mac Low, M.-M., & Heitsch, F. 2004, *ApJ*, 605, 800  
 McKee, C. F. & Ostriker, E. C. 2007, *ARA&A*, 45, 565  
 Miura, A. & Pritchett, P. L. 1982, *J. Geophys. Res.*, 87, 7431  
 Nordlund, Å. & Padoan, P. 1999, in *Interstellar Turbulence*, ed. J. Franco & A. Carramiñana (Cambridge University Press), 218  
 Ostriker, E. C., Stone, J. M., & Gammie, C. F. 2001, *ApJ*, 546, 980  
 Padoan, P. 1995, *MNRAS*, 277, 377  
 Padoan, P., Juvela, M., Goodman, A. A., & Nordlund, Å. 2001, *ApJ*, 553, 227  
 Padoan, P. & Nordlund, Å. 1999, *ApJ*, 526, 279  
 Padoan, P. & Nordlund, Å. 2002, *ApJ*, 576, 870  
 —. 2004, *ApJ*, 617, 559  
 Padoan, P., Nordlund, Å., & Jones, B. 1997, *MNRAS*, 288, 145  
 Ryu, D., Jones, T. W., & Frank, A. 2000, *ApJ*, 545, 475  
 Tamburro, D., Rix, H.-W., Leroy, A. K., Low, M.-M. M., Walter, F., Kennicutt, R. C., Brinks, E., & de Blok, W. J. G. 2009, *AJ*, 137, 4424  
 Troland, T. H. & Crutcher, R. M. 2008, *ApJ*, 680, 457  
 Vázquez-Semadeni, E. 1994, *ApJ*, 423, 681  
 Vázquez-Semadeni, E., Ballesteros-Paredes, J., & Klessen, R. S. 2003, *ApJ*, 585, L131  
 Vázquez-Semadeni, E., Kim, J., & Ballesteros-Paredes, J. 2005, *ApJ*, 630, L49  
 Wang, H. & George, W. K. 2002, *Journal of Fluid Mechanics*, 459, 429  
 Williams, J. P. & McKee, C. F. 1997, *ApJ*, 476, 166  
 Zuckerman, B. & Palmer, P. 1974, *ARA&A*, 12, 279